submitted to *Geophysical Journal International* (April 5, 2002)

Thermodynamic constraints on seismic inversions

N.M. Shapiro and M.H. Ritzwoller

Center for Imaging the Earth's Interior

Department of Physics, University of Colorado at Boulder

Boulder, CO 80309-0390, USA

nshapiro@ciei.colorado.edu, ritzwoller@ciei.colorado.edu

SUMMARY

We discuss two types of physical constraints derived from thermodynamics that can be usefully applied during seismic inversions. The first constraint involves assimilating heat-flow measurements in seismic inversions. This can improve seismic models beneath continents, particularly beneath cratons and continental platforms where uncertainties in the heat flow measurements and the crustal radioactive heat production are smallest. The second thermodynamic constraint involves replacing ad-hoc seismic parameterizations by explicitly estimating parameters in the solution of the differential equations that model the thermal state and evolution of the oceanic upper mantle. The thermodynamic model consists of a shallow conductive layer underlain by a convective mantle. This constraint produces more plausible models of the oceanic lithosphere and asthenosphere and reduces the uncertainty of the seismic model while negligibly degrading the fit to the seismic data.

1 INTRODUCTION

As with any inverse problem, seismic tomography suffers from limitations dictated by the distribution and quality of seismic data, as well as trade-offs between diverse structures within the earth. Phrased differently, it is likely that the earth possesses a substantial component in the "null-space" of any realistic number and mix of seismic data (e.g., Deal & Nolet 1996). Regularization methods (e.g., Tikhonov, Occam's inversion and so forth) are designed to control the over-interpretation of data, but do not guarantee the physical acceptability of the resulting model nor a model that lies "near to" the real earth in model space. These limitations are fundamental. To produce more realistic, physically acceptable earth models requires physical constraints to be applied during seismic tomography.

In this paper we discuss two types of physical constraints derived from thermodynamics that can be usefully applied during seismic inversions. The first is the assimilation of heat flow information in the seismic inversion. The second physical constraint imposes theoretical limits on the shape of the temperature curve with depth by explicitly specifying the differential equations that model the thermal state and evolution of the upper mantle and considering only the solutions to these equations. Relating mantle temperatures to seismic velocities is central to the application of both constraints that we consider. There are uncertainties in this relation as well as the physical parameters needed to combine seismic and heat flow data. Application of these physical constraints, therefore, requires quantifying uncertainties and tracking them in the inversion along with the intrinsic uncertainties in the seismic parameters.

To facilitate the error propagation, we perform a Monte-Carlo inversion. The seismic data are surface wave dispersion maps of broad-band group and phase speeds. The group velocity measurements were made at the University of Colorado at Boulder (e.g., Ritzwoller & Levshin 1998; Ritzwoller et al. 2001) and the phase velocity data were donated by Harvard University and Utrecht University (Trampert & Woodhouse 1995; Ekström et al. 1997; Ekström & Dziewonski 1998). The inversion is divided into two steps. The first step is surface-wave tomography (e.g., Barmin et al. 2001; Ritzwoller et al. 2002) in which the measured dispersion curves are inverted to produce 2-D maps of the geographical distribution of phase and group speeds for individual periods and wave-types. The dispersion maps are found with "diffraction tomography", based on a physical model of the surface wave Fresnel zone that accounts for path-length dependent sensitivity, wavefront healing and associated diffraction effects. As a result, we estimate at each geographical location four dispersion curves: the phase velocity of Rayleigh and Love waves at periods between 40 and 150 s, and group velocities between 16 s and 200 s period. In the second step, on a $2^\circ \times 2^\circ$ grid worldwide, these four dispersion curves are inverted to obtain a local radially anisotropic shear-velocity model using a Monte-Carlo method (Shapiro & Ritzwoller 2002), as illustrated in Figure 1. We randomly generate a large number of models and select only those models that fit the observed dispersion curves acceptably. This method is fully non-linear and results in an ensemble of models from which we estimate model uncertainty.

The application of the thermal constraints in the seismic inversion involves a straightforward modification to the Monte-Carlo sampling, as illustrated in Figure 2. Heat flow observations and theoretical constraints on temperature are used to delimit the range of physically plausible temperature models which is then converted into the range of physically plausible seismic models. The Monte-Carlo method randomly samples the models within this range and identifies the subset of the seismic models that acceptably satisfy the seismic data. By reconverting the seismic velocities back into temperature, the ensemble of acceptable temperature models is identified.

Heat flow measurements are most numerous for continents, so we will discuss assimilation of these data in seismic inversions only at continental locations. The theoretical constraints on the mantle temperature profile involve explicitly estimating parameters in the solution of the differential equations that model the thermal state of the upper mantle. The thermal evolution of the oceanic mantle is probably best understood, and we will explicate this method with application only to the oceanic lithosphere.

The method we propose ultimately emerges as a hypothesis test to determine whether the seismic data are consistent with the thermal constraints. If they are consistent, we show that in some cases the range of acceptable seismic models can be substantially reduced, producing smaller uncertainties and presumably a better model. In addition, the model that we estimate is fundamentally a temperature model, which may be closer to what is desired in many cases than the intrinsic seismic speeds. There have been numerous previous studies that have explored the relationship between seismic velocity, temperature, and composition (e.g., Yan et al. 1989; Furlong et al. 1995; Goes et al. 2000; Röhm et al. 2000; Trampert et al. 2001; van Wijk et al. 2001). Recent work has concentrated on estimating variations in temperature and perhaps composition at the length-scales of seismic tomography. Our approach is the converse of most of these earlier studies. We aim to improve the tomography by applying information about temperature and heat flow to ensure the physical reasonableness of the seismic model.

In section 2, we describe the relation between the seismic velocities and the temperatures in the upper mantle and attempt to characterize the uncertainties in this conversion. The heat-flow constraint, with examples in several continental regions, is discussed in section 3. In section 4, we investigate the application of thermodynamic constraints on the sub-oceanic upper mantle.

2 CONVERSION BETWEEN SEISMIC VELOCITIES AND TEMPERATURE IN THE UPPER MANTLE

Converting between seismic velocities and thermodynamic parameters, such as temperature and pressure, has been the subject of numerous studies (e.g. Duffy & Anderson 1989; Sobolev et al. 1996; Goes et al. 2000). Here, we use the method of Goes et al. (2000) where the isotropic seismic velocities are converted to temperatures and vice versa based on laboratory measured thermoelastic properties of mantle minerals and on models of the average mineralogical composition of the mantle beneath different tectonic provinces. We summarize the salient aspects of this procedure in Appendix A. The key issue is to attempt to track uncertainties in the conversion, which we discuss further here.

2.1 Uncertainties associated with temperature-velocity conversion

Uncertainties in the seismic velocity-temperature relationship result from a number of sources, including uncertainties in the thermoelastic properties of individual minerals, uncertainties in mantle composition, and uncertainties in the anelastic correction. The properties of principal mantle minerals are measured in laboratories with quite high precision and, therefore, uncertainties in these parameters are not major contributors to errors in the velocity-temperature conversion. The most important uncertainties relate to mantle mineralogical composition and the anelastic correction.

2.1.1 Uncertainties in mantle composition

Variations in mantle composition between different tectonic and geological provinces are roughly constrained by studies of mantle xenoliths (e.g., McDonough & Rudnick 1998). A prominent compositional heterogeneity within continents is the difference between the depleted on-cratonic mantle and the off-cratonic mantle (Table 1). Seismic velocities at 60 km depth computed using these two different compositions are shown in Figure 3. Compositional uncertainties have strongest effect at low temperatures, and affect P-wave speed more than S-wave speed in an absolute sense. The velocities computed with these two compositions differ by no more than about 2%. Compositional variations within a single tectonic regime are expected to be smaller and we conservatively estimate the uncertainty in the velocity-temperature conversion caused by composition to be about 1%.

2.1.2 Uncertainties in the anelastic correction

The anelastic properties of mantle materials are not as well constrained by laboratory measurements. Therefore, the anelastic correction is a large source of uncertainties in the temperature-seismic velocity conversion. To quantify the effect of the errors in the anelastic parameters, we calculated seismic velocities for two different values of A in equation (A11). The results for $A = 0.049$ and $A = 0.074$ are shown in Figure 3 with solid and dotted lines, respectively. At 1500 °C, changing A by 50% results in almost a 10% variation of the shear velocity, which means the uncertainties due to the anelastic correction are large at high temperatures, but are probably negligible at temperatures below about 1100 °C.

2.1.3 Other, unmodeled uncertainties

The presence of substantial quantities of melt and/or water in the mantle would affect seismic velocities strongly (e.g., Karato & Jung 1998). Unfortunately, a rigorous quantitative description of these effects does not exist yet. The influence of water and melt probably can be neglected in old continental lithosphere which is believed to be dry due to episodes of melting in the formation of cratons, and too cold for the presence of melt in the uppermost mantle. Because the uncertainty in the anelasticity correction is also small for cold materials, we expect that the temperature-velocity relation works better in old continental areas, while the uncertainties in this relation are largest in regions that have undergone recent lithospheric rejuvenation.

3 APPLICATION OF THE HEAT-FLOW CONSTRAINT BENEATH CONTINENTS

Surface heat flow is correlated with surface tectonics, both within continents and oceans. In oceans, average heat flow decreases with increasing sea-floor age as a result of the cooling of the oceanic lithosphere (e.g., Stein & Stein 1992). A similar pattern is observed in continents where heat flow is lowest for the Archean cratons (e.g., Nyblade & Pollak 1993; Rudnick et al. 1998). This global correlation suggests a relation between the surface heat flow and the thermal regime of the upper mantle. This relation is less straightforward in continents where it is masked by the distribution of the radioactive heat production in the continental crust (e.g., Nyblade & Pollak 1993).

Various researchers have used heat-flow observations to infer the thermal structure of the continental lithosphere (e.g., Artemieva & Mooney 2001; Russell et al. 2001). These inversions require a-priori information on the distribution of the radioactive heat production in the crust and often are based on some simplifications to the thermal equation. Given that the errors in the heat-flow measurements can be large and the distribution of the crustal heat production is poorly known, uncertainties in heat-flow inversions tend to be large.

Information about the thermal structure of the mantle derived from heat flow data is complementary to information obtained from seismic data contained within a seismic model. In some previous studies, the geotherms predicted from the seismic models were compared with those predicted from heat flow observations (e.g., Röhm et al. 2000; Goes et al. 2000). Here, we propose the next step, to use heat-flow measurements as additional data to constrain the seismic model. The key question is if the uncertainty in temperature estimated from the heat flow data is smaller than the uncertainty estimated from the seismic model. If it is smaller, the heat-flow constraint would be useful to improve the seismic inversion. Therefore, estimating uncertainties in both the seismic and the heat-flow inversions is crucial to combine heat-flow and seismic data.

The estimation of uncertainties in the seismic surface wave inversion performed with a Monte-Carlo method is described by Shapiro & Ritzwoller (2002). Here, our discussion will concentrate on estimating the uncertainties in the heat flow inversion. Because of the nature of the thermal equation, this uncertainty grows with depth, so we limit the objective of the heat-flow inversion to constrain just one parameter in our model; namely, the temperature (or seismic velocity) at the top of the mantle. Deeper structures are estimated from seismic data alone.

3.1 Constraining temperature at the top of the mantle with heat-flow data

We assume that the thermal structure of the crust can be approximated by the steady-state solution of the 1-D thermal conductivity equation (B5) with boundary conditions (B4) and (B6). If the surface heat flow q_0, the distribution of internal heat production $H(z)$, and thermal conductivity $k(z)$ are known, equation (B5) can be solved for the geotherm $T(z)$. These parameters, however, are known only approximatively, so the estimated temperature is uncertain. To estimate this uncertainty, we consider surface heat flow to lie in the interval $[q_0 - dq_0, q_0 + dq_0]$ and also consider a range of values for the average heat production and thermal conductivity in the crust: $[k_{min}, k_{max}]$ and $[H_{min}, H_{max}]$. Following the properties of the steady-state solutions described in Appendix A2 (Figure A3), we use $q_0 + dq_0$, k_{min}, and H_{min} to compute the higher geotherm, and $q_0 - dq_0$, k_{max}, and H_{max} to compute the lower geotherm. The ranges of allowed values for crustal conductivity and radioactive heat production are taken from Rudnick et al. (1998) and are shown in Table 2.

Figure 4 presents an example of geothermal bounds calculated at two points, one is a stable craton (Siberian craton, 64N 114E) and the other is a tectonically active region (SE Utah, 38N 110W). We take heat-flow measurements by applying a Gaussian spatial smoothing function ($\sigma = 200$ km) to the heat-flow database of Pollack et al. (1993). Uncertainties in the heat-flow measurements are based on differences in average heat flow reported for similar tectonic provinces around the world. Rudnick et al. (1998) report that $dq_0 \sim$10 mW/m^2 for cratonic regions and $dq_0 \sim$17 mW/m^2 for non-cratonic regions. Regional uncertainties will be smaller than these values, and we use uncertainties of $dq_0 \sim$5 mW/m^2 and $dq_0 \sim$10 mW/m^2 for cratonic and non-cratonic regions, respectively. The heat flow measurements used in this paper are summarized in Table 3.

Figure 4 shows that the uncertainty in the temperature estimated from surface heat-flow increases with depth, which is the reason we use heat-flow data only to constrain the temperature at the top of the mantle; i.e., just below the Moho boundary. The location of this boundary is also known with some uncertainty. We use the global model CRUST2.0 (G. Laske, personal communication), which is a refinement of CRUST5.1 (Mooney et al. 1998), as the a-priori model of crustal thickness. We allow a perturbation of the Moho depth of $\pm$5 km. Extreme geotherms combined with the range of allowed Moho depths define an area of allowed temperatures at the top of the mantle as shown in Figure 4. The uncertainty in the estimated temperature is significantly smaller beneath cratons than tectonically deformed regions because (1) there are smaller uncertainties in the thermal parameters in cratonic than in non-cratonic regions and (2) the lower temperatures in cratonic regions are less sensitive to uncertainties in the anelastic behavior of mantle materials (Figure 3). The heat-flow constraint, therefore, will be most useful in stable continental areas.

3.2 Constraining the shear velocity at the top of the mantle

Using the temperature-velocity relation described by equations (A1)-(A13) and illustrated in Figure 3, the areas of allowed temperatures can be converted to areas of allowed shear velocities at the top of the mantle. The results for two points are shown in Figure 5. As with temperatures, heat-flow data produce much stricter bounds on the shear velocities in cratonic areas than in active tectonic areas

3.3 Surface wave inversion constrained by heat-flow data

We apply the heat flow constraint during the Monte-Carlo inversion of surface wave dispersion using the area of allowed shear velocities at the top of the mantle. Only the models with sub-Moho velocities lying inside the allowed area are considered to be acceptable.

To test the usefulness of the heat flow constraint, we consider four locations (Table 3); two in cratonic regions (Siberian craton, Russian platform) and two in regions that have undergone recent tectonic deformation (Southern Germany, Southeastern Utah). Results of the surface wave inversion in the Siberian craton with and without the heat flow constraint are shown in Figure 6. The heat flow constraint significantly reduces the range of acceptable seismic models. A similar result is obtained for the Russian platform (Figure 7). In tectonic regions, the heat flow constraint is not as useful. In Southern Germany (Figure 8), the constraint slightly reduces the uncertainty of the seismic model while in Southeastern Utah (Figure 9), it has no effect at all. In Southeastern Utah, the temperature bounds that emerge from the heat-flow constraint are broader than the ensemble of seismic models defined by the seismic data alone.

In conclusion, heat flow data are useful to improve seismic models in cratons or continental platforms. In tectonic continental regions, uncertainties in the heat flow information may be larger than the intrinsic uncertainties in the seismic models derived from seismic data alone. The heat flow constraint could also be applied in oceanic areas. Because of the simple structure and thinness of the oceanic crust, the uncertainty associated with the heat-flow constraint in oceans is expected to be smaller than in continental areas. This awaits further exploration as databases of oceanic heat-flow measurements develop.

4 THERMAL STRUCTURE OF THE OCEANIC LITHOSPHERE

As we show, seismic models of the oceanic lithosphere would benefit from constraints to ensure physical plausibility. The physical constraints we apply are based on a simple physical model of heat transfer in the oceanic upper mantle shown in Figure 10 in which a conductive layer is underlain by a convective mantle. This thermodynamical model is effected by a thermal parameterization which is simply the solution to the differential equations that represent conductive and convective cooling in each layer smoothly joined by a transition region.

4.1 Ad-hoc seismic parameterization of the oceanic upper mantle

Figures 11a-c show the results of the surface wave inversion at a point in the Southern Pacific (44S 134W) where lithospheric age is ~48 Ma (Mueller et al. 1997). Figures 11d-f show similar results for a point in the Northern Pacific (32N 160W) where lithospheric age is ~ 101 Ma. Several non-physical features are apparent in the inferred temperature profiles, particularly in Figure 11f. Examples are the constant average temperature between depths of 20 and 40 km and the temperature decrease below 200 km. These problems are partially caused by the ad-hoc nature of the seismic basis functions which are not designed specifically to model temperature anomalies in the oceanic upper mantle. In fact, the cubic B-spline parameterization used by Shapiro & Ritzwoller (2002) apparently over-parameterizes the oceanic upper mantle, resulting in non-physical vertical oscillations that are only apparent when one inspects the temperatures inferred from the seismic model. Figure 12 shows the difference between randomly selected members of the ensemble of acceptable models beneath the Northern Pacific location, displaying these vertical oscillations. Differences between the acceptable models are unconstrained by the Monte-Carlo inversion and, therefore, are in the null-space of the seismic data.

Another problem in oceanic regions with the seismic parameterization used by Shapiro and Ritzwoller (2002) is a fixed P−to−S velocity ratio. This has no significant effect on relatively deep structures because surface waves are not sensitive to P−wave velocities at large depths. However, the Rayleigh waves have non-negligible sensitivity to v_p down to about one eight of a wavelength (e.g., Dahlen & Tromp 1998); i.e., to the P−wave speed in the crust and the upper part of the oceanic lithosphere at long periods. As a consequence, unrealistic P−to−S velocity scaling can affect the result of the inversion at depths less than 50 km. Finally, it is also necessary to apply stronger constraints on the crustal structure than during the inversion described by Shapiro & Ritzwoller (2002) which was oriented more toward continental areas where strong variations in the crustal structure are more likely.

These considerations together motivate the application of physical constraints on the seismic model beneath oceans. Presumably similar problems exist beneath continents as well.

4.2 Thermal parameterization of the oceanic upper mantle

To overcome the artifacts of ad-hoc seismic parameterizations, we explicitly apply thermodynamic constraints on the allowed shear velocities by developing a physically motivated parameterization. The idea is to parameterize the thermal structure of the upper mantle in terms of solutions to the differential equations consistent with the model shown in Figure 10, and then to convert the thermal model into $P-$ and $S-$wave velocities using equations (A1)-(A13).

We assume that heat transfer in the shallow part of the upper mantle is controlled by conduction. This conductive layer is separated from the convective mantle by a transition layer. The temperature profile within the conductive layer is described by the half-space cooling solution given by equation (B7). Following Appendix B, we fix the mantle temperature $T_m = 1300°$C and describe the conductive part of the model with one parameter; i.e., cooling age τ_c. We consider the conductive and convective layers to be thermally decoupled, which implies that the parameters describing these two layers are independent. In the convective layer, we fix the adiabatic thermal gradient D_a to 0.5°C/km (Turcotte & Schubert 1982) and the free parameter is the potential temperature T_p (Appendix B). The transition layer provides a smooth transition between the conductive and convective parts of the model. The thicknesses of the conductive and the transition layer depend on the cooling age. The bottom of the conductive layer is defined as the depth at which the temperature calculated with equation (B7) is equal to 1100°C. The thickness of the transition layer is set to 70% of the thickness of the conductive layer.

The mantle temperature profile, therefore, is described by only two parameters: the cooling age τ_c and the potential temperature in the convective mantle T_p. These two paramters replace the four cubic B-splines used by Shapiro & Ritzwoller (2002). Figure 13 shows the temperature and the shear velocity quality factor predicted by such a simple thermal model with $T_p = 1300°$C for four different cooling ages. The temperature decreases and the quality factor increases with increasing cooling age. The value of the quality factor predicted for the asthenosphere beneath the young ocean is consistent with existing observations (e.g., Canas & Mitchell 1981; Chan et al. 1989).

Results of the inversion using the thermal parameterization are shown in Figure 14 for the same two points in the Pacific shown in Figure 10. Comparison of the inversions using the thermal and the seismic parameterizations (Figures 14 and 11) reveals that, while there is no significant difference in the misfit to the observed dispersion curves, the inversion with the thermal parameterization has several distinct advantages. First, the non-physical artifacts disappear from the temperature profiles. Temperature increases monotonically with depth. Second, the uncertainties in seismic velocities and temperatures are significantly reduced. Third, the parameters used in the thermal parameterization are more convenient for interpretation than the spline coefficients used in the ad-hoc seismic parameterization. For example, consider the estimated range of cooling ages. At the point in the Southern Pacific (44S 134W), τ_c ranges between 33 Ma and 63 Ma and the lithospheric age (48 Ma) lies within these bounds. However, at the Northen Pacific point (32N 160W), the estimated cooling age is systematically lower than the age of the lithosphere (40-72 Ma compared with 101 Ma). This result agrees with the lithospheric flattening of old lithosphere (e.g., Parsons & Slater 1977; Stein & Stein 1992). An advantage of using the thermal parameterization is that the estimated cooling age with uncertainties results directly from the Monte-Carlo inversion.

5 DISCUSSION

We discussed the application of two types of thermodynamic constraints applied in the inversion of seismic surface wave data. First, we considered how heat-flow measurements can be used to improve seismic models beneath continents. Our results show that the uncertainties in the heat flow measurements and the crustal radioactive heat production are small enough in cratonic areas to ensure that the heat-flow constraint is useful. In tectonic areas, however, the uncertainties in temperature estimated from the heat flow data may be too large to improve the seismic models. It is likely that the heat-flow constraint also will be useful in oceanic areas wherever reliable heat-flow measurements exist because complications related to the crust are less important in oceans.

The second thermodynamic constraint involves explicitly solving for parameters in the solution of the differential equations that model the thermal state and evolution of the upper mantle. The main idea is to parameterize the temperature profile in terms of these solutions and then to convert to seismic velocities. We develop this thermal parameterization for the oceanic upper mantle consisting of a shallow conductive layer underlain by a convective mantle with an adiabatic temperature gradient. The temperature profile within the conductive layer is taken from a cooling half-space. The inversion with the thermal parameterization produces more plausible models and reduces the uncertainty of the seismic model while the fit to the observations remains about the same as the inversion with a purely ad-hoc seismic parameterization. As Figure 15 illustrates, similar thermal parameterizations may be warranted for the continental lithosphere.

We believe that these constraints, when applied systematically, will improve upper mantle seismic models, at least beneath cratons and continental platforms and for the oceanic lithosphere. Further efforts in the development of a heat flow data base (including crustal radioactive heat production and thermal conductivity) are justified, therefore, at least in non-tectonic areas, and may be needed before the systematic application of the heat flow constraint. Systematic application of the theoretical constraint on the shape of the temperature profile in the oceanic mantle is more straightforward, however. An example is presented in Figure 16, which shows that substantial variability in the oceanic lithosphere that appears with an ad-hoc seismic parameterization is questionable on physical grounds and is not needed to fit the seismic data. Similar thermal modeling can be performed in subduction zones, as the subducting lithosphere heats up as it penetrates into the mantle. At least in motivation, this application would be similar to previous work by Spencer & Gubbins (1980), Deal et al. (1999), and Deal & Nolet (1999).

Table 1. Mineralogical composition used for the upper mantle (e.g., Dick et al. 1984; McDonough & Rudnick 1998).

	Olivine (%)	Orthopyroxene (%)	Clinopyroxene (%)	Garnet (%)	Spinel (%)	X_{Fe}
On-cratonic	83	15	0	2	0	0.086
Off-cratonic	68	18	11	3	0	0.1
Oceanic	75	21	3.5	0	0.5	0.1

Table 2. Thermal parameters of the crust and upper mantle (e.g., Turcotte & Schubert 1982; Rudnick et al. 1998; Artemieva & Mooney 2001).

	Q (μWm^{-3})	k (Wm^{-1}K^{-1})	κ (m^{2}s^{-1})
Cratonic crust	0.3-0.7	2.5-3.0	1×10^{-6}
Off-cratonic crust	0.4-1.4	2.5-3.0	1×10^{-6}
Upper mantle	0.0	4.0	1×10^{-6}

Table 3. Heat flow values, taken from Pollack et al. (1993), at the four locations considered.

Location	Lat	Lon	q_0 (mWm^{-2})	dq_0 (mWm^{-2})
Siberian craton	64N	114E	25	5
Russian platform	64N	40E	37.5	5
Southern Germany	50N	10E	70	10
Southeastern Utah	38N	110W	80	10

APPENDIX A: CONVERSION BETWEEN TEMPERATURE AND SEISMIC VELOCITIES

A1 Anharmonicity

We consider the mantle to be composed of five principal minerals: olivine, orthopyroxene, clinopyroxene, garnet, and spinel. For each mineral, we calculate the elastic moduli μ and K and density ρ as functions of temperature T, pressure P, and iron content X based on the following equations:

$$\mu(P,T,X) = \mu_0 + (T - T_0)\frac{\partial \mu}{\partial T} + (P - P_0)\frac{\partial \mu}{\partial P} + X\frac{\partial \mu}{\partial X} \tag{A1}$$

$$K(P,T,X) = K_0 + (T - T_0)\frac{\partial K}{\partial T} + (P - P_0)\frac{\partial K}{\partial P} + X\frac{\partial K}{\partial X} \tag{A2}$$

$$\rho(P,T,X) = \rho_0(X)\left[1 - \alpha(T - T_0) + \frac{(P - P_0)}{K}\right] \tag{A3}$$

$$\rho_0(X) = \rho_0|_{X=0}\frac{\partial \rho}{\partial X} \tag{A4}$$

$$\alpha(T) = \alpha_0 + \alpha_1 T + \alpha_2 T^{-1} + \alpha_3 T^{-2} \tag{A5}$$

The coefficient of thermal expansion is denoted by α and the subscript 0 refers to the values of a quantity at the $P-T$ condition at the Earth's surface with zero iron content. The following quantities and their partial derivatives are defined from laboratory experiments (see Goes et al. (2000) for a summary):

$$\rho_0|_{X=0}, \mu_0, K_0, \frac{\partial \rho}{\partial X}, \frac{\partial \mu}{\partial X}, \frac{\partial K}{\partial X}, \frac{\partial \rho}{\partial T}, \frac{\partial \mu}{\partial T}, \frac{\partial K}{\partial T}, \frac{\partial \rho}{\partial P}, \frac{\partial \mu}{\partial P}, \frac{\partial K}{\partial P}, \alpha_0, \alpha_1, \alpha_2, \alpha_3 \tag{A6}$$

The average elastic moduli and density for a given mantle composition are calculated based on volumetric proportions of individual minerals λ_i and the Voigt-Reuss-Hill averaging scheme:

$$\langle \rho \rangle = \sum \lambda_i \rho_i \tag{A7}$$

$$\langle \mu \rangle = \frac{1}{2}\left[\sum \lambda_i \mu_i + \left(\frac{\lambda_i}{\mu_i}\right)^{-1}\right] \tag{A8}$$

$$\langle K \rangle = \frac{1}{2}\left[\sum \lambda_i K_i + \left(\frac{\lambda_i}{K_i}\right)^{-1}\right] \tag{A9}$$

With the following standard relations

$$v_p = \sqrt{K + \frac{4}{3}\mu/\rho} \qquad\qquad v_s = \sqrt{\mu/\rho} \tag{A10}$$

we obtain seismic velocities as functions of iron content, mineralogical composition, temperature, and pressure, which is equivalent to depth if we neglect lateral pressure variations.

A2 Anelasticity

Anharmonic effects represent only one part of the temperature-velocity relation. At high mantle temperatures, anelasticity contributes significantly (e.g., Karato 1993). The anelastic behavior of mantle materials results in the attenuation of seismic waves and also affects the seismic velocities. Its effect is generally described in terms of the quality factor Q. We use the mantle attenuation model of Minister & Anderson (1981) in which shear quality factor within an absorption band is written as a function of temperature and pressure:

$$Q_\mu(P,T,\omega) = A\omega^a exp(a(H^* + PV^*)/RT) \tag{A11}$$

where A and a are constants, H^* is the activation energy, V^* is the activation volume, and ω is frequency. During the surface-wave inversion, the velocity model is produced at unit frequency, therefore $\omega = 2\pi$. The $P-$wave quality factor is

$$Q_P = \frac{3}{4}\frac{v_s^2}{v_p^2} Q_\mu \tag{A12}$$

The velocity correction associated with anelastic attenuation is performed in the following way:

$$v_{anel}(P,T,\omega) = v(P,T,\omega)\left[1 - \frac{2Q^{-1}(P,T,\omega)}{\tan(\pi a/2)}\right] \tag{A13}$$

where v is v_p or $v-s$ and Q is Q_μ or Q_P, respectively. As shown in Figure A1, this correction becomes less than one percent for $Q > 200$. Following Sobolev et al. (1996), we use $a = 0.15$, $H^* = 500$ kJ/mol, and $V^* = 2.0 \times 10^{-5}$ m^3/mol. However, we re-calibrated the constant A. Sobolev et al. (1996) calibrated their attenuation model to fit certain measurements of the seismic quality factor and found $A = 0.148$. We prefer to calibrate the anelastic correction based on seismic velocity measurements and use our global model (Shapiro & Ritzwoller 2002), which has an average shear velocity of 4.4 km/s at 200 km depth. With an average mantle temperature at this depth of 1400°C, to fit this shear velocity we obtain $A \sim 0.049$. This value of A tends to reduce Q and strengthens the anelastic correction.

APPENDIX B: THERMAL MODEL OF THE CRUST AND THE UPPER MANTLE

Below the Earth's surface, the temperature increases rapidly with depth. As a consequence, the viscosity decreases very rapidly with depth in the shallow part of the upper mantle. This strong viscosity gradient results in different regimes of heat transfer. In the high-viscosity lithosphere, heat transfer is dominated by conduction while convective heat transfer is more effective in the deeper part of the mantle with lower viscosity.

B1 Convective Mantle

If convection occurs adiabatically, the temperature in the convective part of the upper mantle increases approximately linearly with depth z (Figure A2):

$$T = T_p + D_a z \tag{B1}$$

where T_p is the potential temperature and D_a is the adiabatic gradient that can be expressed as (e.g., Turcotte & Schubert 1982):

$$D_a = \frac{\alpha g T_a}{c_p} \tag{B2}$$

where α is the coefficient of thermal expansion, T_a is the average temperature of the convective upper mantle, g is the acceleration of gravity, and c_p is the specific heat.

B2 Conductive Lithosphere

If we neglect lateral temperature variations, the temperature inside the lithosphere is controlled by the 1D thermal conductivity equation:

$$\frac{\partial T}{\partial t} = \kappa \frac{\partial^2 T}{\partial z^2} + \frac{\kappa}{k} H \tag{B3}$$

with the boundary condition

$$T|_{z=0} = 0 \tag{B4}$$

where κ is the thermal diffusivity (set to 1.0×10^{-6} m^2/s), T is temperature, t is time, z is depth, H is the volumetric heat production, and k is thermal conductivity.

We consider two types of solutions of this thermal equation. The first is the steady-state solution when the temporal derivative in (B3) equals zero and the conductivity equation becomes:

$$\frac{\partial^2 T(z)}{\partial z^2} = -H(z)/k(z) \tag{B5}$$

In a stationary regime, the constant surface heat flow, q_0, results in an additional boundary condition:

$$q_0 = k\frac{\partial T}{\partial z}|_{z=0} \tag{B6}$$

The solution of equation (B5) with boundary conditions (B4 and B6) depends on three parameters: the surface heat flow q_0, the radioactive heat production H, and the thermal conductivity k. As shown in Figure A3, higher heat-flow implies higher mantle temperatures, while higher heat production and thermal conductivity implies in lower temperatures if heat flow is held constant.

We also consider a time-dependent "cooling" solution of equation (B3). In this case, the initial condition is a constant temperature T_m. The cooling solution depends on this initial mantle temperature T_m, the time of cooling called here the cooling age τ_c, and the thermal conductivity and the thermal diffusivity and the heat production in the crust and in the upper mantle. In the general case, the solution of the equation (B3) can be easily found numerically. However, in the simplest case of a homogeneous half-space without internal heat production the cooling solution takes a simple analytical form known as the half-space cooling model (e.g., Turcotte & Schubert 1982):

$$T(z) = T_s + (T_m - T_s)\ \mathrm{erf}\left(\frac{z}{2\sqrt{\kappa\tau_c}}\right), \tag{B7}$$

where T_s is the surface temperature. This model can be reasonably applied to the oceanic lithosphere where the radioactive heat production is very low and the the crust is very thin. If we fix the mantle thermal diffusivity, the half-space cooling solution depends on two parameters: τ_c and T_m. However, these two parameters are not completely independent. Figure A4 shows two half-space cooling temperature profiles, one with the a cooling age $\tau_c = 90$

Ma and mantle temperature $T_m = 1300$ °C and the other with $\tau_c = 110$ Ma and $T_m = 1400$ °C. These profiles are nearly indistinguishable at low temperatures (<1100 °C) where the the heat transfer is expected to be conductive. This low-temperature part of the profile can be represented with a variety of combinations of τ_c and T_m because larger thermal ages can be compensated by increased mantle temperatures.

ACKNOWLEDGMENTS

The application of heat flow as a constraint in the seismic inversion was inspired by conversations with Walter Mooney. We are grateful to Shijie Zhong for numerous discussions and to Irina Artemieva for providing us with the results of her heat flow inversions at an early stage of her research. We are also particularly grateful to Jeannot Trampert at Utrecht University and Michael Antolik, Adam Dziewonski, and Goran Ekström at Harvard University for providing phase velocity measurements. Gabi Laske provided CRUST2.0 prior to publication. All maps were generated with the Generic Mapping Tools (GMT) data processing and display package (Wessel and Smith, 1991, 1995). Aspects of this work were supported by grants from the Office of Polar Programs at the U.S. National Science Foundation, NSF-OPP-9615139 and NSF-OPP-9818498, and Defense Threat Reduction Agency contracts DTRA01-99-C-0019 and DTRA01-00-C-0013.

REFERENCES

Artemieva, I.M. and Mooney, W.D., 2001. Thermal thickness and evolution of Precambrian lithosphere: A global study, *J. geophys. Res.,* **106**, 16,387-16,414.

Barmin, M.P., Ritzwoller, M.H., & Levshin, A.L., 2001. A fast an reliable method for surface wave tomography, *Pure appl. Geophys.*,**158**, 1351-1375.

Canas, J.A. & Mitchell, B.J., 1981. Rayleigh-wave attenuation and its variation across the Atlantic ocean, *Geophys. J. R. astr. Soc.,* **67**, 159-176.

Chan, W.W., Sacks, I.S., & Morrow, R., 1989. Anelasticity of the Iceland plateau from surface wave analysis, *J. geophys. Res.,* **94**, 5675-5688.

Dahlen, F.A. & Tromp, J., 1998. *Theoretical Global Seismology*, Princeton University Press, Princeton, New Jersey.

Deal, M.M. & Nolet, G., 1996. Nullspace shuttles, *Geophys. J. Int.,* **124**, 372-380.

Deal, M.M., Nolet, G., & van der Hilst, R.D., 1999. Slab temperature and thickness from seismic tomography 1. Method and application to Tonga, *J. geophys. Res.,* **104**, 28,789-28,802.

Deal, M.M. & Nolet, G., 1999. Slab temperature and thickness from seismic tomography 2. Izu-Bonin, Japan, and Kuril subduction zones, *J. geophys. Res.,* **104**, 28,803-28,812.

Dick, H.J.B., Fisher, R.L., & Bryan, W.B., 1984. Mineralogic variability of the uppermost mantle along mid-oceanic ridges, *Earth planet. Sci. Lett.,* **69**, 88-106.

Duffy, T.S. & Anderson, D.L., 1989. Seismic velocities in mantle minerals and the mineralogy of the upper mantle, *J. geophys. Res.,* **94**, 1895-1912.

Ekström, G. & Dziewonski, A.M., 1998. The unique anisotropy of the Pacific upper mantle, *Nature*, **394**, 168-172.

Ekström, G., Tromp, J., & Larson, E.W.F., 1997. Measurements and global models of surface waves propagation, *J. geophys. Res.,* **102**, 8137-8157.

Furlong, K.P., Spakman, W., and Wortel, R., 1995. Thermal structure of the continental lithosphere: constraints from seismic tomography, *Tectonophys.*, **244**, 107-117.

Goes, S., Govers, R., & Vacher, R., 2000. Shallow mantle temperatures under Europe from P and S wave tomography, *J. geophys. Res.,* **105**, 11,153-11,169.

Karato, S., 1993. Importance of anelasticity in the interpretation of seismic tomography, *Geophys. Res. Lett.,* **20**, 1623-1626.

Karato, S. & Jung, H., 1998. Water, partial melting and the origin of the seismic low velocity and high attenuation zone in the upper mantle, *Earth planet. Sci. Lett.,* **157**, 193-207.

Kennett, B.L.N., Engdahl, E.R., & Buland, R., 1995. Constraints on seismic velocities in the Earth from travel times, *Geophys. J. Int.,* **122**, 403-416.

McDonough, W.F. & Rudnick, R.L., 1998. *Mineralogy and composition of the upper mantle*, in: Ultrahigh-pressure mineralogy: physics and chemistry of the Earth's deep interior, R.J. Hemley, Editor, Mineralogical Society of America, Washington, DC.

Minister, J.B. & Anderson, D.L., 1981. A model of dislocation-controlled rheology for the mantle, *Philos. Trans. R. Soc. London*, **299**, 319-356.

Mooney, W.D., Laske, G., & Masters, G., 1998. CRUST5.1: A global crustal model at $5° \times 5°$, *J. geophys. Res.,* **103**, 727-747.

Mueller, R.D., W.R. Roest, J.-Y. Royer, L.M. Gahagan, and J.G. Sclater, 1997. Digital isochrons of the world's ocean floor, *J. geophys. Res.,* **102**, 3211-3214.

Nyblade, A.A. & Pollack, H.N., 1993. A global analysis of heat flow from Precambrian terrains: implications for the thermal structure of Archean and Proterozoic lithosphere, *J. geophys. Res.,* **98**, 12,207-12,218.

Parsons, B. & Slater, J.G., 1977. An analysis of the variation of ocean floor bathymetry with age, *J. geophys. Res.,* **82**, 803-827.

Pollack, H.N., Hurter, S.J., & Johnson, J.R., 1993. Heat flow from the Earth's interior: analysis of the global data set *Revs. Geophys.*, **31**, 267-280.

Ritzwoller, M.H. & Levshin, A.L., 1998. Eurasian surface wave tomography: Group velocities, *J. geophys. Res.,* **103**, 4839-4878.

Ritzwoller, M.H., Shapiro, N.M., Levshin, A.L. and Leahy, G.M., 2001. The structure of the crust and upper mantle beneath Antarctica and the surrounding oceans, *J. geophys. Res.,* **106**B12), 30645 - 30670.

Ritzwoller, M.H., Shapiro, N.M., Barmin, M.P., & Levshin, A.L., 2002. Global surface wave diffraction tomography, *J. geophys. Res.,* submitted.

Röhm, A.H.E., Snieder, R., Goes, S., & Trampert, J., 2000. Thermal structure of continental upper mantle inferred from $S-$wave velocity and surface heat flow, *Earth planet. Sci. Lett.,* **181**, 395-407.

Rudnick, R.L., McDonough, W.F., & O'Connell, R.J., 1998. Thermal structure, thickness and composition of continental lithosphere, *Chemical Geology*, **145**, 395-411.

Russell, J.K., Dipple, G.M., & Kopylova, M.G., 2001. Heat production and heat flow in the mantle lithosphere, Slave craton, Canada, *Phys. Earth planet. Inter.,* **123**, 27-44.

Shapiro, N.M. & Ritzwoller, M.H., 2002. Monte-Carlo inversion for a global shear velocity model of the crust and upper mantle. *Geophys. J. Int.,* in press.

Sobolev, S.V., Zeyen, H., Stoll, G., Werling, F., Altherr, R., & Fuchs, K., 1996. Upper mantle temperatures from teleseismic tomography of French Massif Central including effects of composition, mineral reactions, anharmonicity, anelasticity and partial melt. *Earth planet. Sci. Lett.,* **157**, 193-207.

Spencer, C. & Gubbins, D., 1980. Travel-time inversion for simultaneous earthquake location and velocity structure determination in laterally varying media, *Geophys. J. R. astr. Soc.,* **63**, 95-116.

Stein, C.A. & Stein, S., 1992. A model for the global variation in oceanic depth and heat flow with lithospheric age, *Nature*, **359**, 123-129.

Trampert, J. & Woodhouse, J.H., 1995. Global phase velocity maps of Love and Rayleigh waves between 40 and 150 s period, *Geophys. J. Int.,* **122**, 675-690.

Trampert, J., Vacher, P., and Vlaar, N., 2001., Sensitivities of seismic velocities to temperature, pressure, and composition of the lower mantle, *Phys. Earth planet. Inter.,* **124**, 255-267.

Turcotte, D.L. & G. Schubert, 1982. *Geodynamics. Applications of continuum physics to geological problems*, John Wiley & Sons, Princeton, New York.

van Wijk, J.W., Govers, R., and K.P. Furlong, 2001. Three-dimensional thermal modeling of the California upper mantle: a slab window vs. stalled slab, *Earth planet. Sci. Lett.,* **186**, 175-186.

Wessel, P., and W.H.F. Smith, 1991. Free software helps map and display data, *EOS, Trans. Am. geophys. Un., 72*, 441.

Wessel, P., and W.H.F. Smith, 1995. New version of the Generic Mapping Tools released, *EOS, Trans. Am. geophys. Un., 76*, 329.

Lateral variations in upper mantle thermal structure inferred fromn three-dimensional seismic inversion models, *Geophys. Res. Lett.,* **16**, 449-452.

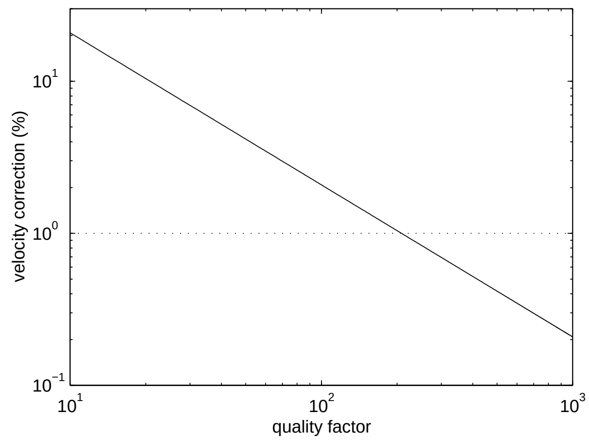

Figure A1. Anelastic velocity correction as predicted by equation (A13).

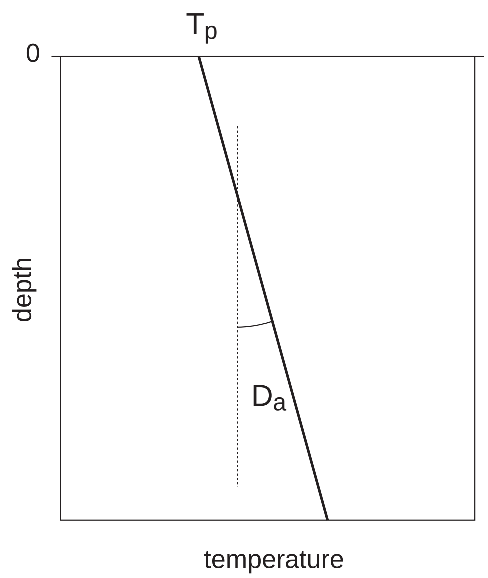

Figure A2. Schematic geotherm in the convective mantle (see equation B1).

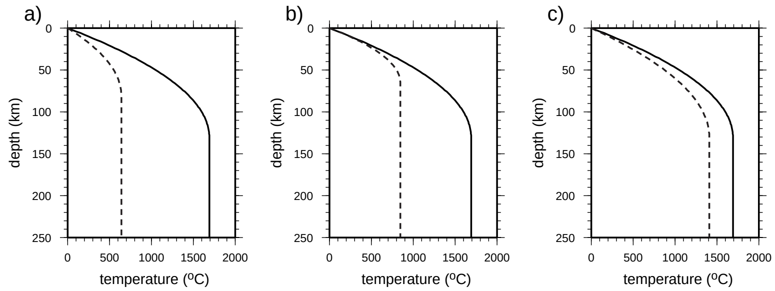

Figure A3. Solutions of the 1D thermal steady-state equation (B5) with boundary conditions (B4 and B6). (a) Effect of surface heat flow. Solid and dashed lines show solutions obtained with $Q_0 = 65$ mW/m^2 and $Q_0 = 40$ mW/m^2, respectively. In both cases, $H = 0.5$ μW /m^3 and $k = 2.7$ Wm^{-1}K^{-1}. (b) Effect of internal heat production. Solid and dashed lines show solutions obtained with $H = 0.5$ μW /m^3 and $H = 1.0$ μW /m^3, respectively. In both cases, $Q_0 = 65$ mW/m^2 and $k = 2.7$ Wm^{-1}K^{-1}. (c) Effect of thermal conductivity. Solid and dashed lines show solutions obtained with $k = 2.7$ Wm^{-1}K^{-1} and $k = 3.0$ Wm^{-1}K^{-1}, respectively. In both cases, $Q_0 = 65$ mW/m^2 and $H = 0.5$ μW /m^3.

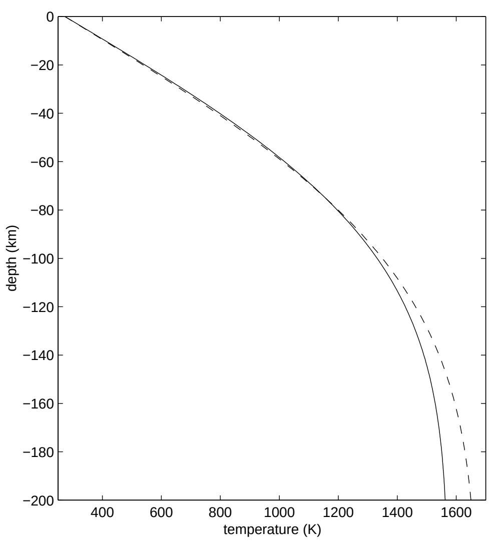

Figure A4. Half-space cooling models (equation B7) with different cooling ages τ_c and mantle temperatures T_M. Solid line corresponds to $T_m = 1300$ °C and $\tau_c = 90$ Ma, and dashed line corresponds to $T_m = 1400$ °C and $\tau_c = 110$ Ma.

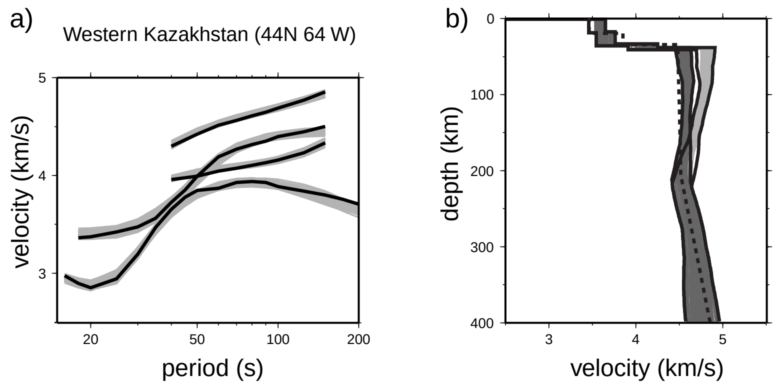

Figure 1. Results of the inversion for an ensemble of acceptable shear velocity models at a point in Western Kazakhstan (44 N, 64 E) using an ad-hoc seismic parameterization. (a) Four dispersion curves obtained from surface wave velocity maps (thick black lines) and the predictions from the ensemble of acceptable models (gray lines). (b) The ensemble of acceptable radially anisotropic models, where v_{sv} and v_{sh} are and shown with dark and light gray shades, respectively. The corridor of acceptable values is indicated with the solid black lines, and the 1-D model ak135 (Kennett et al. 1995) is plotted as the dashed line for reference.

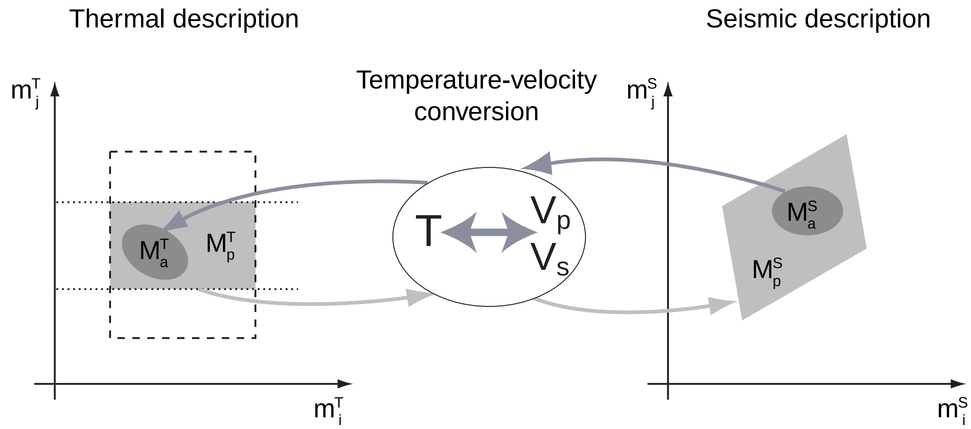

Figure 2. Schematic representation of the Monte-Carlo seismic inversion based on a thermal description of the model. The thermal description (left panel) is constrained by the heat-flow data (horizontal dotted lines) and theoretical constraints on the thermal structure and evolution of the mantle (dashed rectangle). These constraints delimit the range of physically plausible thermal models M_p^T (light shadowed area on the left panel). Using a temperature-seismic velocity conversion, this range is converted into a range of physically plausible seismic models M_p^S (light shadowed area on the right panel). Random sampling within M_p^S identifies the ensemble of acceptable seismic models M_a^S (dark shadowed area on the right panel). Finally, this ensemble is converted into the ensemble of acceptable thermal models M_a^T (dark shadowed area on the left panel).

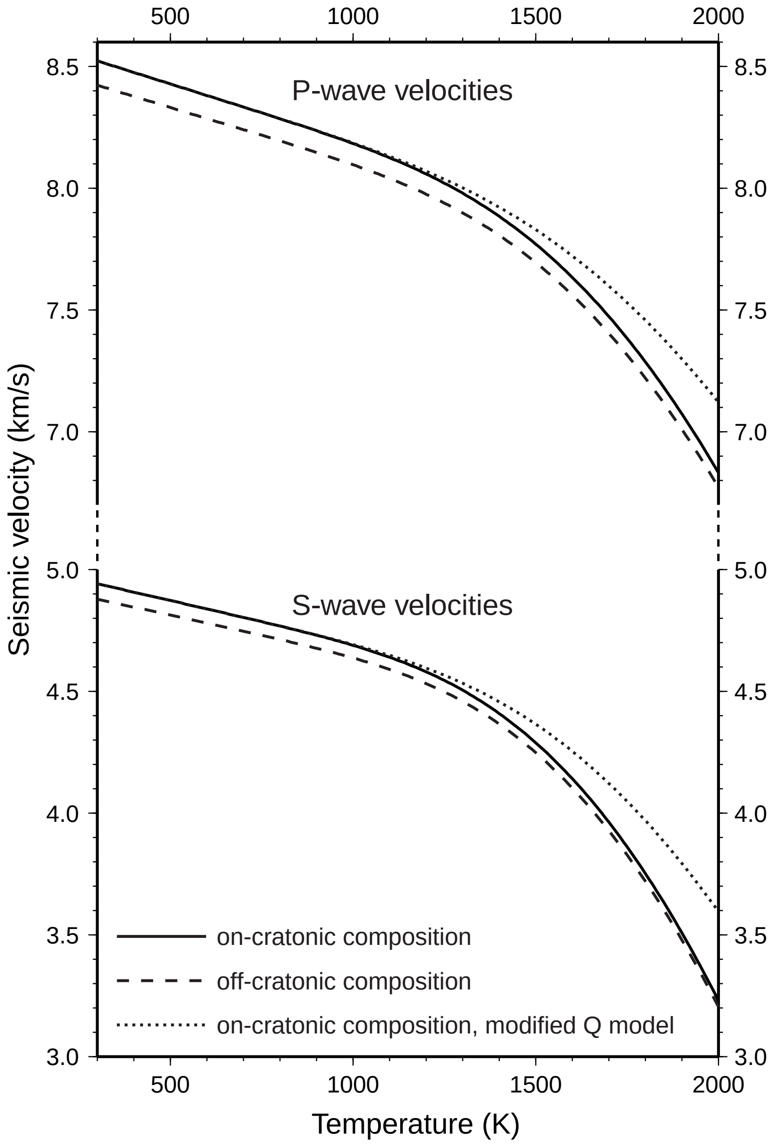

Figure 3. $P-$ and $S-$wave velocities calculated at 60 km depth using equations (A1)-(A13). Solid lines show the results for on-cratonic composition with the "normal" anelastic correction ($A = 0.049$). Dashed lines show the results for the off-cratonic composition with the "normal" anelastic correction. Dotted lines are the results for the on-cratonic composition with a "reduced" anelastic correction ($A = 0.074$).

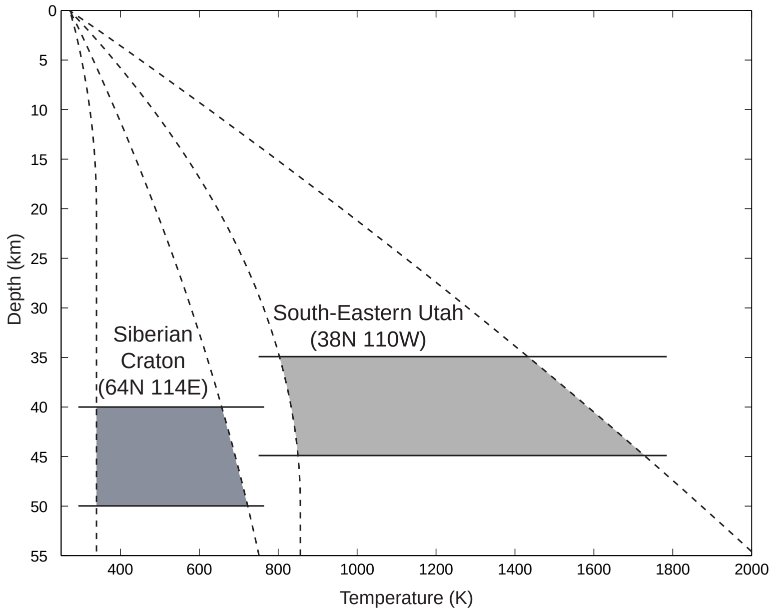

Figure 4. Heat flow constraints on the temperature at the top of the mantle calculated with equation (B5) and boundary conditions (B4 and B6) at two points: (1) the Siberian craton (40N 114E) and (2) Southeastern Utah (38N 110W). The values of the heat flow and crustal thermal parameters are presented in Tables 2 and 3. Dashed lines show extreme geotherms. Horizontal solid lines show the allowed range of Moho depths (CRUST2.0 ± 5 km). Shaded areas define the regions of allowed temperatures at the top of the mantle.

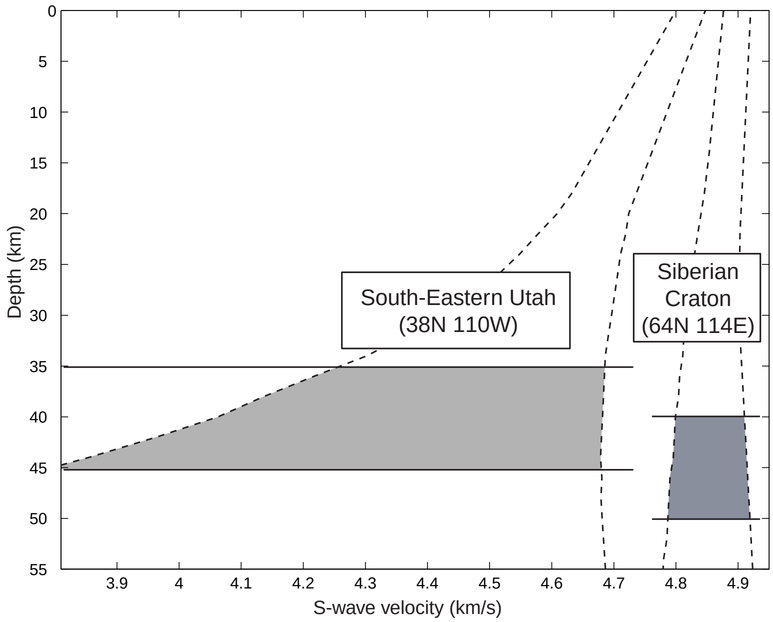

Figure 5. Similar to Figure 4, but for the Heat flow constraints on the shear velocity at the top of the mantle. Extreme geotherms have been converted into velocity limits (dashed lines) by inverting equations (A1)-(A13).

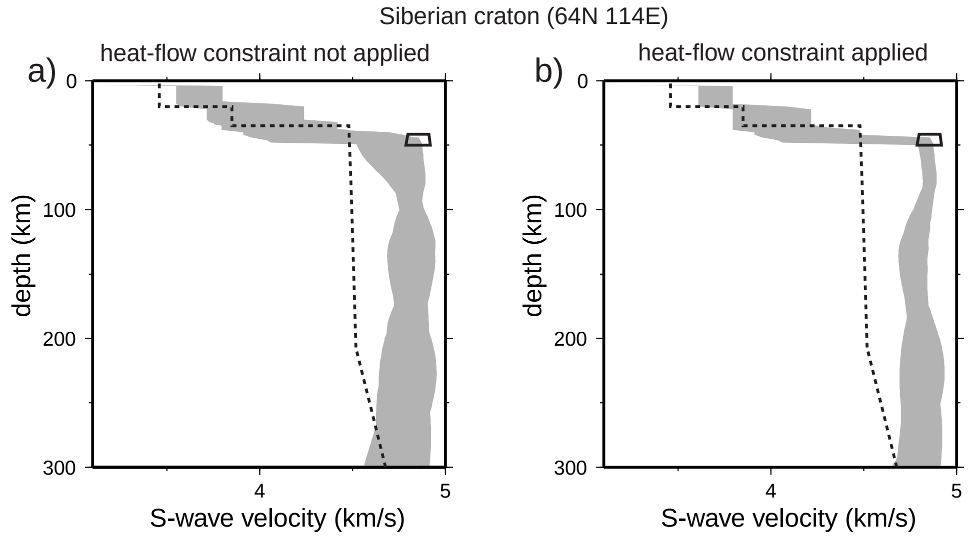

Figure 6. Results of the surface wave inversion at a point in the Siberian craton (64N 114E). The shaded zones identify the ensemble of acceptable models for isotropic shear velocity ($v_s = (v_{sh}+v_{sv})/2$). The dashed lines are the 1-D model ak135 (Kennett et al. 1995), for reference. Black polygons mark the area of allowed shear velocities at the top of the mantle estimated from the heat flow data. (a) Results without the heat-flow constraint. The black polygon is included for reference only. (b) Results with the heat flow constraint. All models pass the the black polygon.

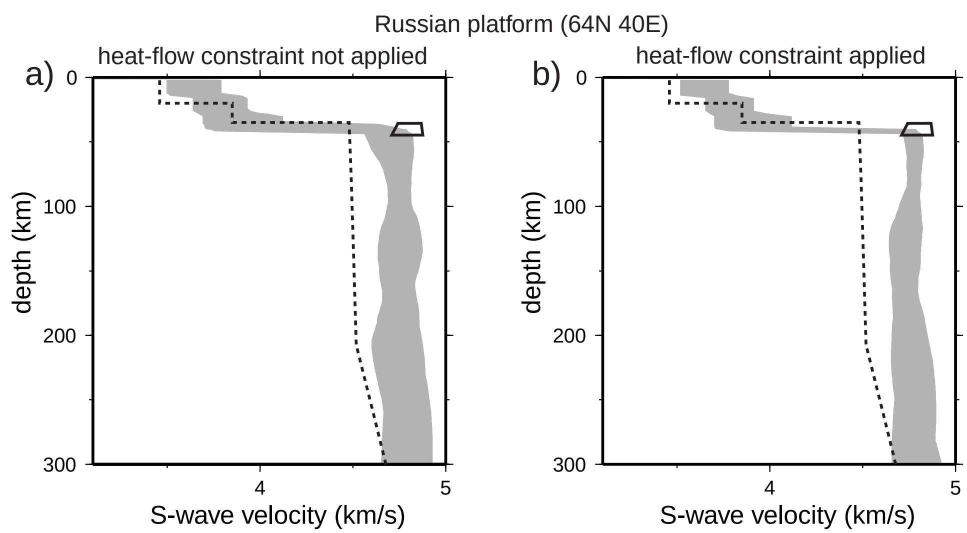

Figure 7. Similar to Figure 6, but for a second cratonic region, the Russian platform (64N 40E).

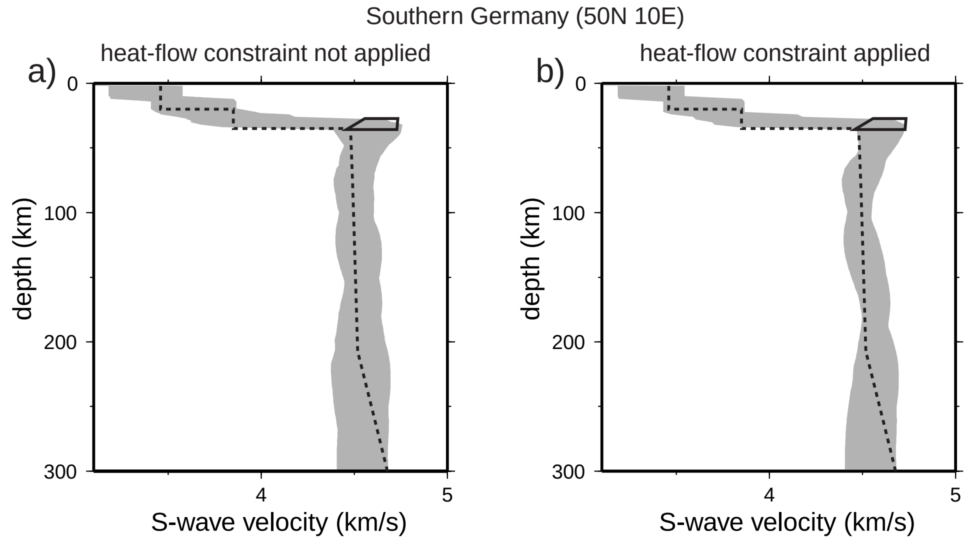

Figure 8. Similar to Figure 6, but for a region that has undergone recent tectonic deformation, a point in Southern Germany (50N 10E).

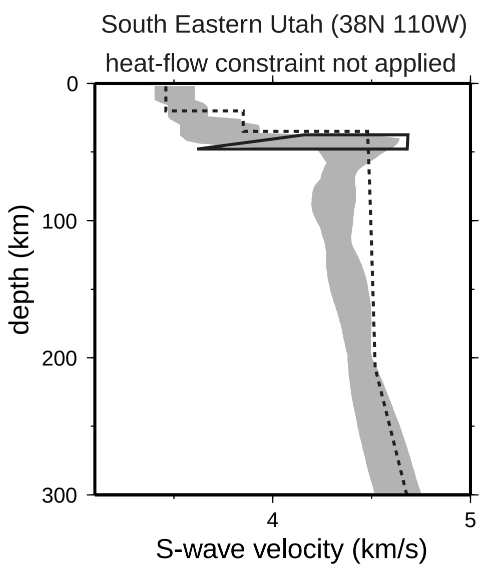

Figure 9. Similar to Figure 6, but for a second region that has undergone recent tectonic deformation, a point in Southeastern Utah (38N 110W). The heat flow constraint does not change the ensemble of acceptable models from those that result from seismic data alone, so only a single panel is shown.

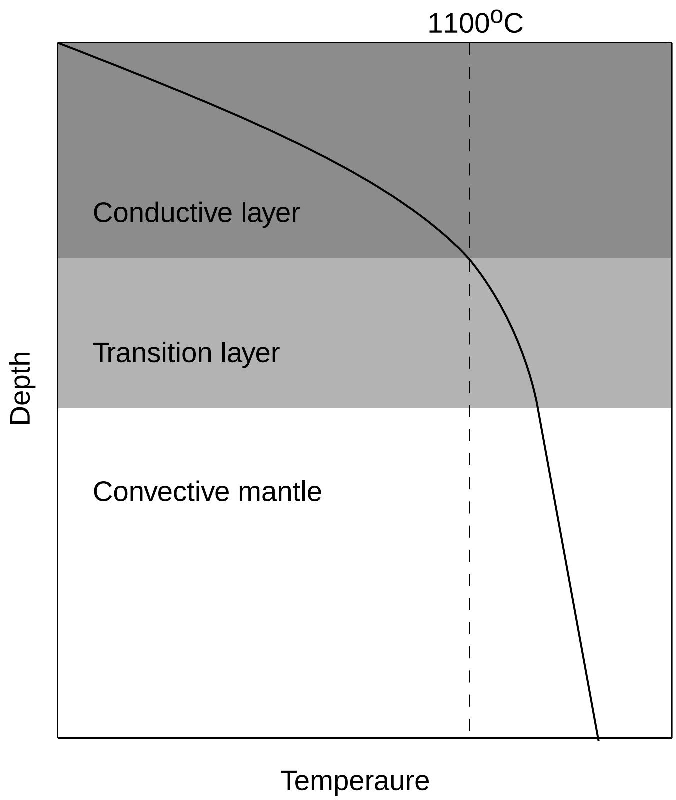

Figure 10. Model of the sub-oceanic upper mantle used to define the thermal parameterization.

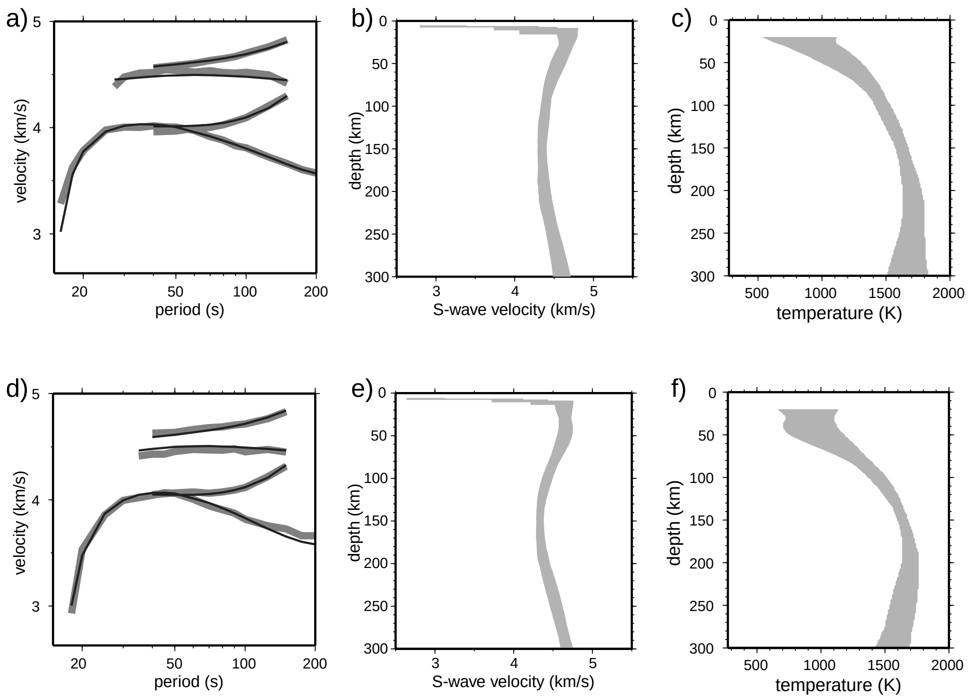

Figure 11. The seismic model and inferred temperature at two points in the Pacific using the ad-hoc seismic parameterization of Shapiro & Ritzwoller (2002). (a-c) Results of the surface-wave inversion for a point in the Southern Pacific Ocean (44S 134W). (a) Dispersion curves, similar to Figure 1a. (b) The shaded area defines the ensemble of acceptable models (isotropic part, $v_s = (v_{sv} + v_{sh})/2$). (c) The shaded area defines the allowed temperatures predicted from the ensemble of acceptable seismic models. (d-f) Similar to (a-c), but for a point in the Northern Pacific (32N 160W).

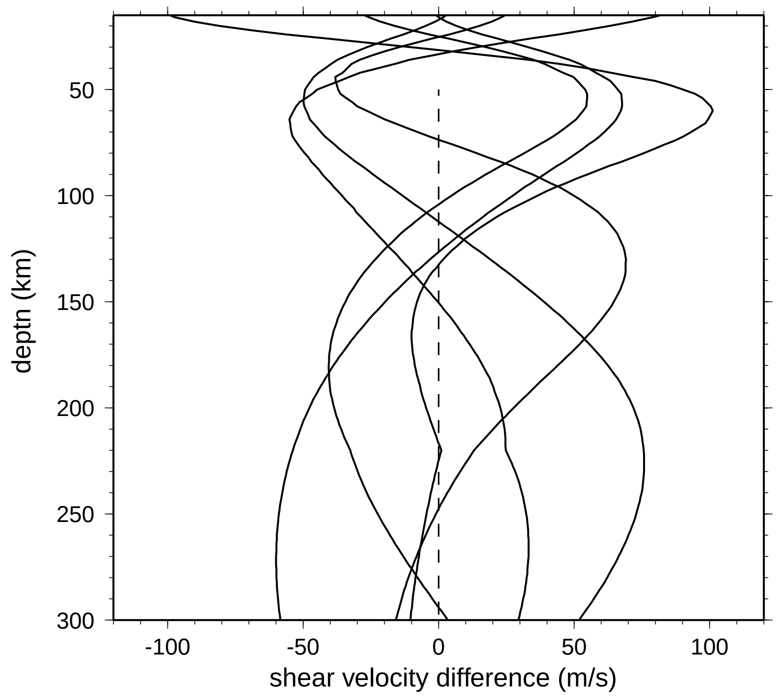

Figure 12. Differences in shear velocities between five randomly selected pairs of acceptable models at the northern Pacific point (32N 160W). These profiles are in the null-space of the data.

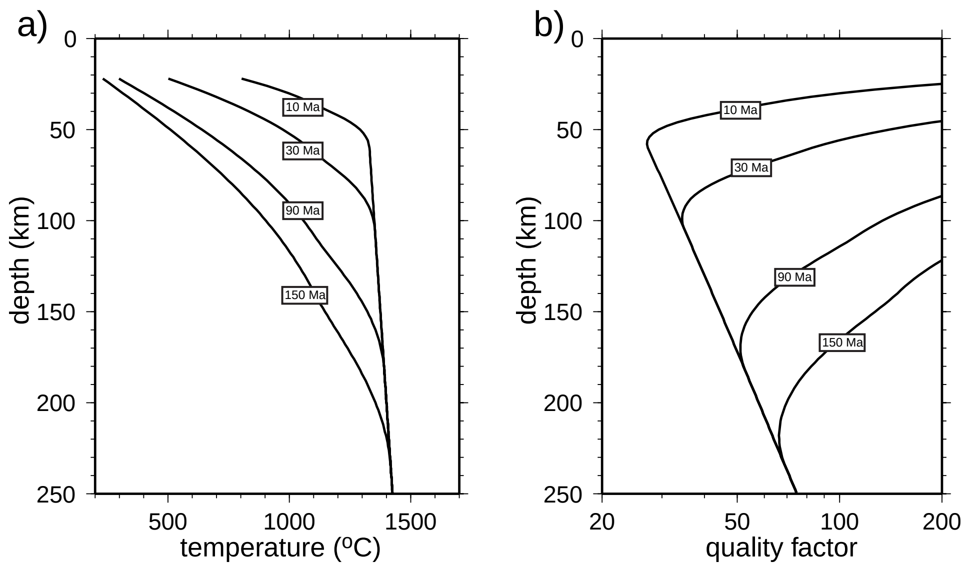

Figure 13. Thermal models of the sub-oceanic upper mantle with the potential temperature $T_p =$ 1300°C and four different cooling ages: 10 Ma, 30 Ma, 90 Ma, and 150 Ma. (a) Temperature as function of depth. (b) Shear quality factor as function of depth.

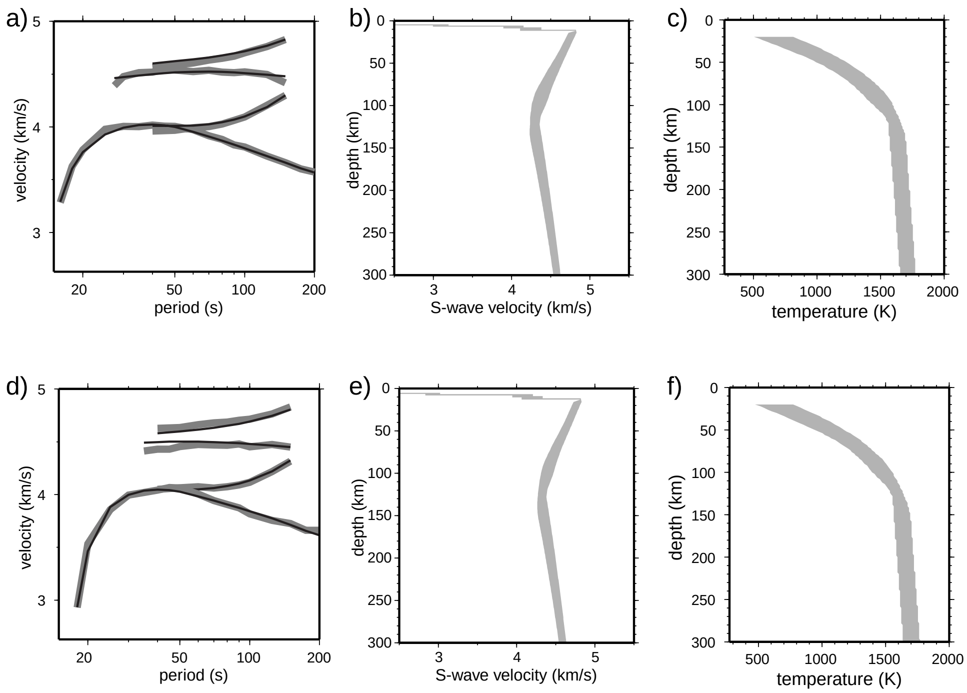

Figure 14. Results of the surface-wave inversion with the thermal parameterization at two points in the Pacific Ocean (44S 134W) and (32N 160W), similar to Figure 11.

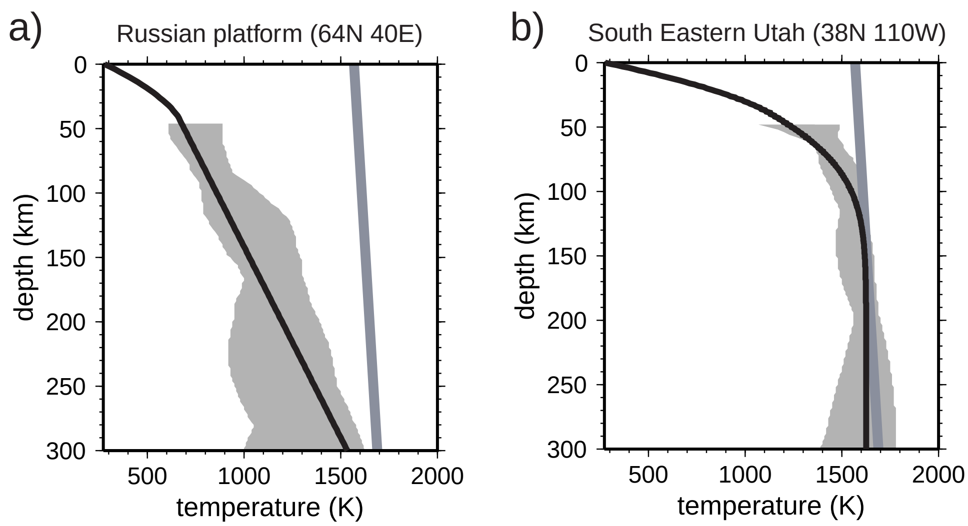

Figure 15. Temperature profiles inferred from the seismic model constrained by heat flow data beneath (a) the Russian Platform (see Figure 7b for the seismic model) and (b) Southeastern Utah (see Figure 9 for the seismic model). The shaded areas define the range of acceptable temperatures at each depth. In (a), the solid black line is the solutions of the 1-D steady-state thermal equation (equation (B5)) and in (b) it is the solution of the 1-D thermal equation (equation (B3)) with a cooling age of 50 Ma. The thick gray lines are the 1300 °C adiabat, for reference.

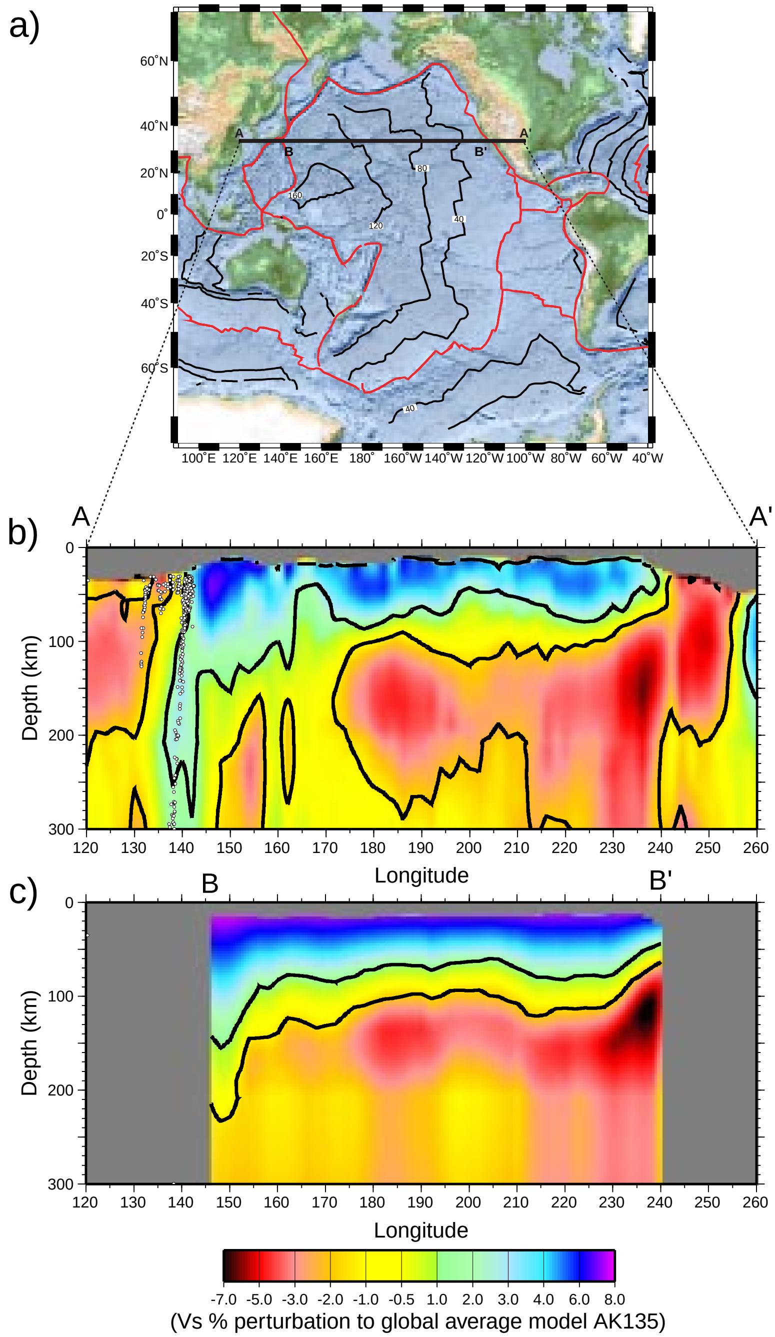

Figure 16. Vertical cross-section across the Pacific along the line indicated in (a), comparing the seismic model obtained with (b) the ad-hoc seismic parameterization of Shapiro & Ritzwoller (2002) and (c) the thermal parameterization in which the thermodynamic constraint on the temperature profile has been applied. Shear speeds are percent perturbation relative to the 1-D model ak135. Black contours enclose the persistent features of each model; i.e., those features that appear in every member of the ensemble of acceptable models.